Response of Subtropical Stationary Waves and Hydrological Extremes to Climate Warming in Boreal Summer

Jiacan Yuan

Department of Earth and Planetary Sciences and Institute of Earth, Ocean and Atmospheric Sciences, Rutgers, The State University of New Jersey, Piscataway, New Jersey

Wenhong Li

Division of Earth and Oceanic Sciences, Nicholas School of the Environment, Duke University, Durham, North Carolina

Robert E Kopp

Department of Earth and Planetary Sciences and Institute of Earth, Ocean and Atmospheric Sciences, Rutgers, The State University of New Jersey, Piscataway, New Jersey

Yi Deng

School of Earth and Atmospheric Sciences, Georgia Institute of Technology, Atlanta, Georgia

ABSTRACT

Subtropical stationary waves may act as an important bridge connecting regional hydrological extremes with global warming. Observations show that the boreal summer stationary-wave amplitude (SWA) had a significantly positive trend during 1979–2013. Here, we investigate the past and future responses of SWA to increasing climate forcing using 31 CMIP5 GCMs. Twenty-four out of 31 models display a consistent increase in climatological-mean SWA in response to warming. To assess the detectability of a trend in SWA, we compared half-century trends between preindustrial control (PiControl), historical, and RCP8.5 simulations. The probability distribution of the normalized SWA trend obtained through bootstrapping shows neither positive nor negative tendencies of SWA trend in PiControl simulations. Twenty-two of 31 historical simulations exhibit a positive SWA trend. The SWA trends in 26 of 31 RCP8.5 simulations are positive. The finding supports the hypothesis that the positive SWA trend is at least partially driven by increasing external forcing. The linear regression of interannual variability in hydrological extreme frequency on SWA suggests that high SWA is related to increased heavy-rainfall-day frequency over South Asia, the Indochinese Peninsula, and southern China (SA-EA), and to increased dry-spell-day frequency over the northwestern and central United States (NUS) and the southern United States and Mexico (SUS-MEX). The projected amplification of SWA, combined with the relationships between SWA and number of hydrological extremes, may partially explain projected increases in the number of dry spells over NUS and SUS-MEX and the number of heavy-rainfall days over SA-EA.

ⓐ Denotes content that is immediately available upon publication as open access.

✎ Supplemental information related to this paper is available at the Journals Online website: https://doi.org/10.1175/JCLI-D-17-0401.s1.

Corresponding author: Jiacan Yuan, jiacan.yuan@gmail.com

1. Introduction

Hydrological extremes (droughts and extreme rainfall events) can cause enormous economic loss and threaten lives. For example, catastrophic flooding in central Europe in June 2013, caused by a 4-day period of heavy precipitation, resulted in an estimated financial cost of more than EUR 12 billion and at least 25 deaths (Grams et al. 2014). Similarly, catastrophic floods in southern

Louisiana in August 2016, due to heavy rainfall within a 72-h period (Vahedifard et al. 2016), led to 13 fatalities and estimated financial damage exceeding $10 billion (U.S. dollars; Aon Benfield 2016).

The frequency of hydrological extremes has increased significantly during recent decades. For example, the global-mean number of heavy precipitation days and fractional contribution of very wet days to total precipitation increased over 1951–2010 (Donat et al. 2013), and the number of record-breaking precipitation events increased globally over 1981–2010 (Lehmann et al. 2015). Droughts have also increased since 1950 over many land areas, including Africa, southern Europe, East and South Asia, and eastern Australia (Dai 2011). These increases can, to a large extent, be explained by a warming climate (Sun et al. 2007).

The moisture content of a warming atmosphere increases according to the Clausius–Clapeyron relationship, contributing to an increase in extreme precipitation (Trenberth et al. 2003; Pall et al. 2007; Zhang et al. 2013). However, the rate of increase in extreme precipitation in general circulation model (GCM) simulations generally does not match the rate of increase in atmospheric moisture content (Pall et al. 2007; Sun et al. 2007). Changes in atmospheric circulation are hypothesized to be another important contributor to precipitation extremes (O'Gorman and Schneider 2009a,b; Lu et al. 2014; Wills et al. 2016).

Numerous recent studies demonstrate that atmospheric stationary waves are a link between global warming and the growing frequency of extreme events (Liu et al. 2012; Petoukhov et al. 2013; Coumou et al. 2014; Screen and Simmonds 2014; Yuan et al. 2015; Mann et al. 2017). Quasi-stationary waves (hereafter stationary waves), which consist of persistent highs and lows in the atmosphere, could shape regional hydroclimate and modify its change (Simpson et al. 2016; Wills and Schneider 2016). Coumou et al. (2014) demonstrated that the amplification of synoptic-scale stationary waves (wavenumbers 6–8) leads to persistent local weather conditions and synchronizes monthly-scale extreme events in midlatitudes. They also argued that Arctic amplification (the phenomenon that surface temperatures increase faster over the Arctic than over lower latitudes; Screen and Simmonds 2014) provides favorable conditions for the resonance mechanisms that stimulate wave amplifications (Petoukhov et al. 2013).

In boreal summer, subtropical stationary waves consist of subtropical high pressure systems over the North Pacific and North Atlantic (Davis et al. 1997; Rodwell and Hoskins 2001; Miyasaka and Nakamura 2005; Li et al. 2011) and monsoonal low pressure systems over Eurasia and North America (Adams and Comrie 1997;

Chen 2003; Holton and Hakim 2012). In principle, they are stationary waves with wavenumber 2 and arise from longitudinal asymmetries in topography, diabatic heating, and transient eddies (Ting 1994; Nigam and DeWeaver 2003). Using reanalysis data and gauge-based observational data, Yuan et al. (2015, hereafter Yuan15) found that these subtropical stationary waves increased in amplitude during recent decades, and this amplification has implications for the subtropical hydrological extremes.

In 2016, global mean surface temperature for 2016 was about 0.9°C higher than its twentieth-century average (NOAA 2017). Between 1986–2005 and 2081–2100, it is projected to increase by 3.7° ± 0.7°C under representative concentration pathway (RCP) 8.5, the highest-forcing RCP, and by 1.0° ± 0.4°C under RCP2.6, the lowest-forcing RCP (Collins et al. 2013). While several recent studies have investigated the influence of warming climate on stationary waves and the hydrological cycle (Levine and Boos 2016; Wills and Schneider 2016), these studies used idealized GCMs without a seasonal cycle or realistic boundary conditions.

Here, we use fully coupled comprehensive GCMs with realistic boundary conditions—specifically, simulations from phase 5 of the Coupled Model Intercomparison Project (CMIP5; Taylor et al. 2012)—to investigate four key questions. First, in comprehensive GCMs, by how much does the amplitude of summer subtropical stationary waves increase in response to forcing? Second, how do forced changes compare to internal variability in the linear trend of stationary-wave amplitude? Third, how do hydrological extremes relate to stationary waves, and how does this relationship change in response to forcing? Fourth, in light of this relationship, how do changes in stationary waves and the relationship between stationary waves and hydrological extremes contribute to projected changes in the number of hydrological extremes in a warming climate?

2. Data and methodology

a. Data

We examine subtropical stationary waves in three different experiments conducted by 31 models (Table 1) from the CMIP5 archive (Taylor et al. 2012). 1) The preindustrial control (PiControl) experiment simulates the unforced, internal variability of the climate system. It holds greenhouse gas concentrations at the preindustrial level. 2) The historical simulation is forced by both anthropogenic and natural forcing from 1850 to 2005. 3) RCP8.5 is a forcing scenario for 2006–2100 that is consistent with high greenhouse gas emissions, such that the radiative forcing in 2100 is about 8.5 W m^{-2}. The

TABLE 1. A list of CMIP5 models used in this study, where the checkmarks indicate the variable is available; U and V are zonal and meridional winds, and Pr is precipitation. (Expansions of acronyms are available online at http://www.ametsoc.org/PubsAcronymList.)

Model	Modeling center	Variables			Latitude of the maximum stationary waves (°N)
		U	V	Pr	
ACCESS1.0	CSIRO-BOM	✔	✔	✔	30
ACCESS1.3		✔	✔		30
CCSM4	NCAR	✔	✔	✔	30
CESM1(BGC)	NSF/DOE NCAR	✔	✔	✔	30
CESM1(CAM5)		✔	✔		30
CMCC-CESM	CMCC	✔	✔		30
CMCC-CM		✔	✔		30
CNRM-CM5	CNRM-CERFACS	✔	✔	✔	32.5
CSIRO-Mk3.6.0	CSIRO-QCCCE	✔	✔	✔	30
CanESM2	CCCma	✔	✔	✔	25
FGOALS-g2	LASG-CESS	✔	✔		30
GFDL-CM3	NOAA GFDL	✔	✔	✔	30
GFDL-ESM2G		✔	✔	✔	30
GFDL-ESM2M		✔	✔	✔	30
GISS-E2-H	NASA GISS	✔	✔		30
GISS-E2-R		✔	✔		30
GISS-E2-R-CC		✔	✔		30
HadGEM2-CC	MOHC	✔	✔		30
HadGEM2-ES		✔	✔		30
IPSL-CM5A-LR	IPSL	✔	✔	✔	30
IPSL-CM5A-MR		✔	✔	✔	27.5
IPSL-CM5B-LR		✔	✔		27.5
MIROC-ESM-CHEM	MIROC	✔	✔	✔	27.5
MIROC-ESM		✔	✔	✔	30
MIROC5		✔	✔	✔	32.5
MPI-ESM-LR	MPI-M	✔	✔	✔	30
MPI-ESM-MR		✔	✔	✔	30
MRI-CGCM3	MRI	✔	✔	✔	30
NorESM1-M	NCC	✔	✔	✔	30
NorESM1-ME		✔	✔		30
BCC-CSM1.1	BCC	✔	✔	✔	30
INM-CM4	INM	✔	✔	✔	30

horizontal resolution of the atmospheric component of the CMIP5 GCMs varies from 0.75° to 3.75°. We use horizontal wind from the model simulation output in Northern Hemisphere summer [June–August (JJA)] to compute the streamfunction for characterizing stationary waves.

To examine hydrological extremes, we do not use the raw precipitation data produced by CMIP5 models because precipitation extremes in the CMIP5 simulations generally have large biases compared to observations (Sillmann et al. 2013; Mehran et al. 2014). Instead, we use statistically bias-corrected and downscaled daily precipitation data from NASA Earth Exchange (NEX) Global Daily Downscaled Projections (GDDP) (Thrasher et al. 2012), for which only 20 of the 31 CMIP5 models (Table 1) in two scenarios (historical and RCP8.5) are available. In this dataset, precipitation is bias corrected with respect to the Global Meteorological Forcing Dataset observational data (Sheffield et al. 2006) and downscaled to a 0.25° × 0.25° grid using

the quantile-mapping-based bias-correction spatial disaggregation method. To examine the portion of the simulations with the largest forced signal, we utilize the data in the last 50 years of each scenario (1956–2005 and 2050–99).

b. Stationary wave amplitude

In Yuan15, subtropical stationary waves were represented by an eddy streamfunction (deviation from the zonal mean) averaged over JJA (Fig. 1a in Yuan15). The streamfunction, a measure of the rotational component of circulation, is used to characterize stationary waves because stationary waves are Rossby waves, which are nearly nondivergent (i.e., the horizontal divergence is much smaller than vorticity). Although previous studies (e.g., Seager et al. 2010; Wills et al. 2016) suggest that changes in divergent circulations are the primary contributor of changes in the hydrological cycle, stationary waves, though nearly nondivergent, can influence the hydrological cycle by altering the vertical motion

through the vorticity balance in the lower troposphere. More specifically, zonal variation of net precipitation primarily results from zonal anomalies of lower-troposphere vertical motion sustained by Ekman pumping and advection of planetary vorticity associated with the large-scale stationary eddy circulations (Wills and Schneider 2015).

Yuan15 used the variance of the 925-hPa streamfunction at 30°N, which is the latitude of the maximum stationary waves, to measure the amplitude of stationary waves (SWA), that is, the intensity of the atmospheric troughs and ridges along the subtropical band. In this study, we apply a similar definition of SWA to summer mean data in every year. To examine the latitude of the maximum stationary waves in each model, we plot the time evolution of streamfunction variance between 15° and 45°N (see Fig. S1 in the online supplemental material). The latitude of the maximum stationary waves varies across models between 27.5° and 32.5°N (see latitudes in Table 1); there is no apparent meridional shift of maximum amplitude observed on decadal time scales. Therefore, we define the SWA for each model as the variance of 925-hPa streamfunction at the latitude of the maximum stationary waves in that model. SWA is measured in stationary wave units (SWU), defined as $10^{13}\,\mathrm{m}^4\,\mathrm{s}^{-2}$. In this study, we use a 50-yr time length to compute the linear trend of SWA because this length is longer than most time periods of internal variability of atmospheric circulation.

c. Hydrological extremes

To measure summer hydrological extremes, we count the number of days in a dry spell and the number of heavy-rainfall days in each summer. A dry spell is defined as an event of at least 3 consecutive days when daily precipitation is less than 1 mm, while a heavy-rainfall day is defined as a day when the precipitation exceeds the 99th percentile of daily precipitation in JJA during the period 1955–2005. We then count the number of dry-spell days and heavy-rainfall days at each grid point during JJA of each year.

3. Results

a. Model climatology of SWA

We first examine the climatological-mean SWA during the last 50 years in each scenario of each model. The median climatological-mean SWA increases from 6.8 to 8.2 SWU between the PiControl and historical simulations, while the increase between the historical and RCP8.5 simulations is smaller (from 8.2 to 8.5 SWU) (Fig. 1a). The spread of SWAs in RCP8.5 is broader than

that in the other two scenarios. In most individual models, with the exceptions of HadGEM2-CC and HadGEM2-ES, SWA increases dramatically from PiControl to historical simulations (Fig. 1b). From historical to RCP8.5 simulations, 26 of 31 models exhibit an increase in climatological-mean SWA (Fig. 1b). In total, SWAs in 24 of 31 models exhibit a consistent increase in mean SWA from PiControl to historical to RCP8.5. The seven exceptions are CMCC-CM, CNRM-CM5, FGOALS-g2, GFDL-ESM2G, GFDL-ESM2M, HadGEM2-CC, and HadGEM2-ES.

b. Linear trend of SWA

A significantly positive linear trend of SWA was observed during 1979–2013 (Yuan15), but it is challenging to distinguish forced responses from unforced variability using observations (Kohyama et al. 2017). Accordingly, to assess if this positive SWA trend is partially driven by recent fast climate warming, we investigate trends of SWA in the PiControl, historical, and RCP8.5 simulations.

To characterize the internal climate variability, we apply a bootstrap method (Efron and Tibshirani 1994) to SWA time series in PiControl simulations. Specifically, we randomly resample thirty 50-yr trends of SWA from each model's PiControl simulation. To standardize the trend values across models, the SWAs from each model are centered around and normalized by the model's PiControl climatological-mean SWA (μ). These normalized trends are reported in units of percent of climatological-mean SWA per decade. From the 31 models, we obtain 930 samples of SWA trend. The resulting probabilistic distribution of the normalized SWA trend is shown in Fig. 2. In PiControl, the sampled distribution of SWA trend ranges from -0.025 to $+0.026\,\mu\,\mathrm{decade}^{-1}$, with a median of 0. Using bin widths of $0.005\,\mu\,\mathrm{decade}^{-1}$, about 36.9% of the samples fall in negative value bins, about 36.9% in positive value bins, and 26.2% in the bin centered at zero (from -0.0025 to $+0.0025\,\mu\,\mathrm{decade}^{-1}$). There is no tendency toward either a positive or a negative trend in unforced simulations.

To investigate the response to anthropogenic forcing, we examine the SWA trend in the last 50 years of historical and RCP8.5 simulations. The spreads of SWA trends across the 31 GCMs are also shown in Fig. 2. The intermodel spread rather than the bootstrap method is used for historical and RCP8.5 simulations because the forcing is not stationary but rather monotonically increasing in these two scenarios. In the historical simulations, the SWA trends range from -0.02 to $+0.04\,\mu\,\mathrm{decade}^{-1}$, with a median of $0.004\,\mu\,\mathrm{decade}^{-1}$. Twenty-two of 31 models exhibit positive SWA trends. In RCP8.5, the spread of SWA trends further extends toward
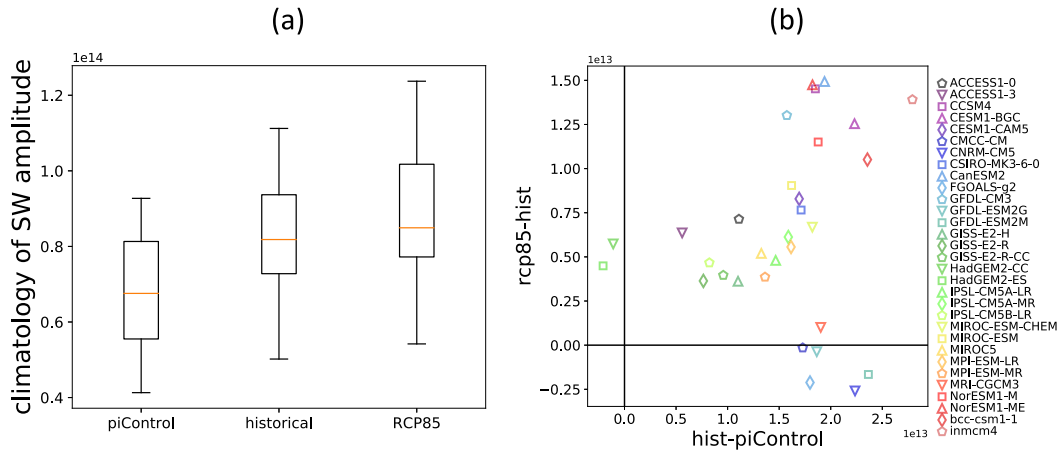
FIG. 1. (a) Multimodel ensemble of 50-yr climatological SWA ($m^4 s^{-2}$) in the PiControl, historical, and RCP8.5 scenarios. Orange lines are median values, boxes mark the 25%–75% likely range, and caps denote the 5%–95% likely range. (b) Difference of climatological SWA between RCP8.5 and historical against that between historical and PiControl. The 31 CMIP5 models are color-indexed. The last 50 years of each scenario are used to compute the climatological SWA.

the positive end, ranging from -0.04 to $+0.07\,\mu\,\mathrm{decade}^{-1}$, with a median of $+0.01\,\mu\,\mathrm{decade}^{-1}$. Positive SWA trends are found in 26 of 31 models.

To test whether the spread of SWA trends in historical or RCP8.5 is consistent with the null hypothesis that these are randomly sampled from the distribution of trends in PiControl, we examine the probability of N positive samples in 31 random draws from the distribution of SWA trends in PiControl, where N is 22 for the historical simulations and 26 for the RCP8.5 simulations.

The probability of 22 (26) positive samples out of 31 random draws from the PiControl distribution is $p = 7.7 \times 10^{-3}$ (5.7×10^{-5}). These results suggest that external forcing makes a positive SWA trend, like that observed during recent decades, more probable.

c. Relationship between hydrological extremes and SWA on an interannual time scale

Yuan15 investigated the relationships between SWA and number of hydrological events using observational
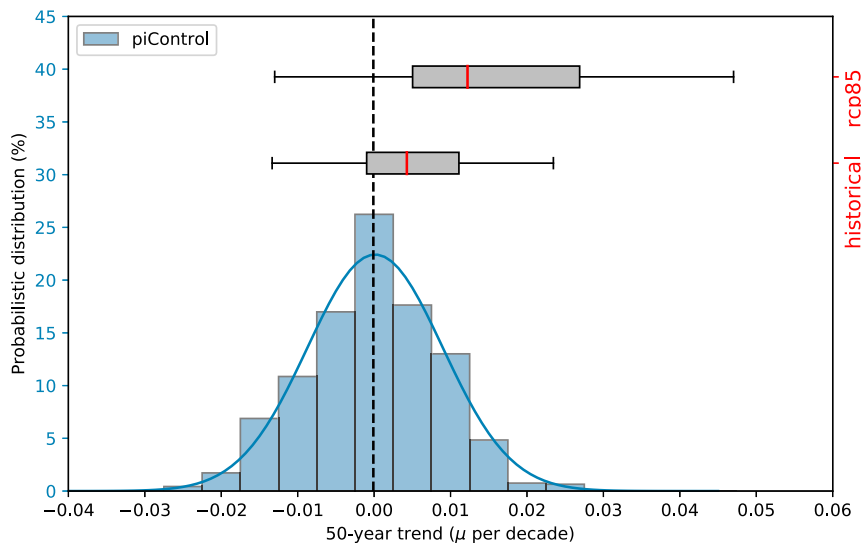

FIG. 2. Probabilistic distribution of the 50-yr trend of stationary wave amplitudes in the PiControl scenario obtained by the bootstrapping method (blue histogram). The blue line is a Gaussian fit of the distribution, and the black dashed line marks the median of the distribution. Boxplots show the intermodel spread of the linear trend of stationary wave amplitudes during the last 50 years of the historical and RCP8.5 scenarios. All these results are obtained from 31 models.
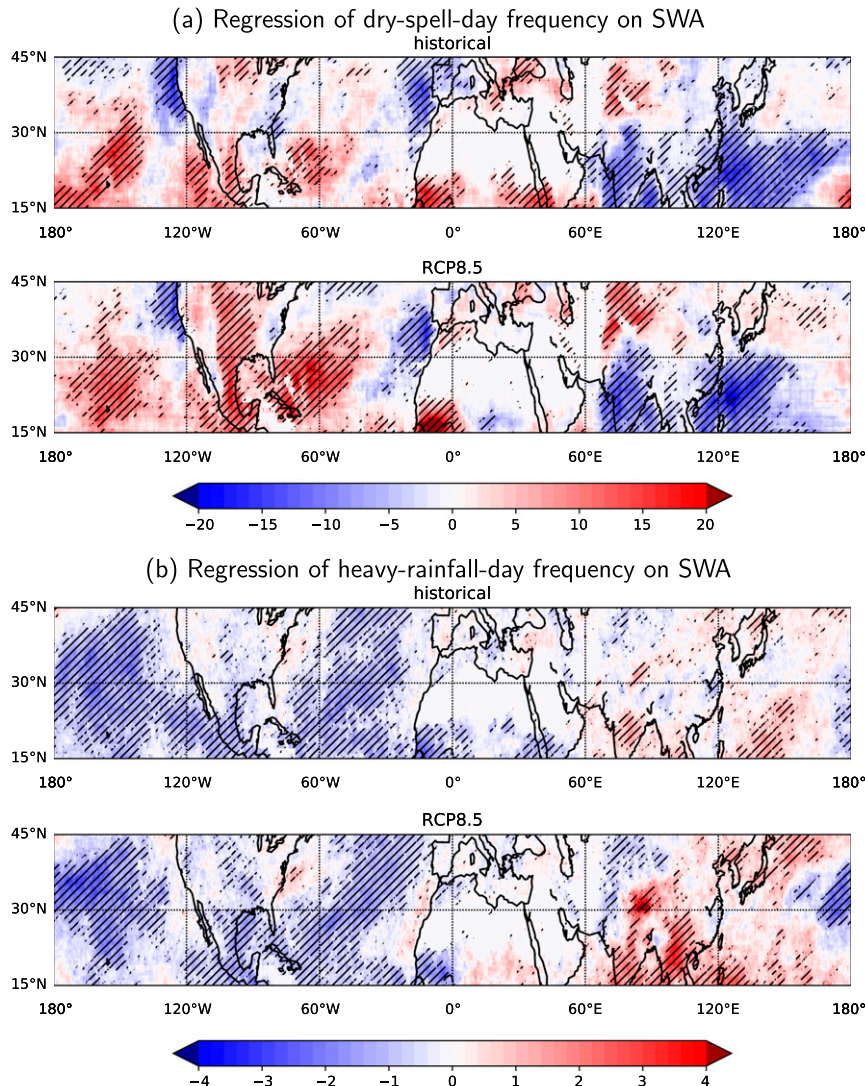
(a) Regression of dry-spell-day frequency on SWA

(b) Regression of heavy-rainfall-day frequency on SWA

FIG. 3. Mean of multimodel ensemble regression coefficient (day μ^{-1}) between SWA and interannual variability in the number of (a) dry-spell days and (b) heavy-rainfall days in historical simulations in the upper panels and RCP8.5 simulations in the lower panels. Warm (cool) colors denote positive (negative) values. Hatched areas denote values significant at the $p < 0.1$ level by the Student's t test.

data. They hypothesized a bridge between the SWA and hydrological extremes: stationary waves over subtropics could influence the number of hydrological extremes through large-scale moisture transport. To assess whether there are relationships between SWA and number of hydrological extremes in forced simulations and how the relationships respond to increased forcing, we examine the relationship between SWA and hydrological extremes in both historical and RCP8.5 scenarios. To do this, we regress the annual number of dry-spell days and heavy-rainfall days on SWA in historical and RCP8.5 simulations (Fig. 3). The regression coefficient

$[R(x, y)]$ for each model is defined as the least squares estimate:

$$n_i(x,y) = R(x,y)(\text{NSWA}_i - \overline{\text{NSWA}_i}) + \overline{n_i(x,y)} + \varepsilon_i, \quad (1)$$

where NSWA denotes the seasonal-average normalized SWA; i indexes years in the temporal sequence of 50 years; n_i denotes the number of days of the hydrological extreme in each year; ε_i denotes a random error, and x and y are longitude and latitude, respectively. The bar indicates the average over the 50 years. The regression coefficients represent, on an interannual time scale, the changes in number of hydrological extremes in JJA

associated with changes in stationary-wave amplitude, which measures the intensity of high pressure systems (anticyclonic flow) and low pressure systems (cyclonic flow) along the subtropical band. For this analysis, we use only the 20 GCMs in which bias-corrected daily precipitation is available in NASA-NEX-GDDP. The multimodel mean of regression coefficient is shown in Fig. 3.

In general, the regression coefficients of dry-spell-day frequency have larger amplitude than those of heavy-rainfall-day frequency. In the historical simulations, higher SWA is associated with increased dry-spell-day frequency over Mexico, the midwestern United States, the Sahel, and central Asia, and with decreased dry-spell frequency over South Asia, the Indochinese Peninsula, and southern China (Fig. 3a). The pattern of regression coefficient of dry-spell-day frequency in RCP8.5 is similar to that in the historical simulations, except that the magnitude of coefficients is amplified over some regions (i.e., the positive coefficients increase over Mexico, the central United States, Mauritania, and central Asia, and the negative coefficients increase over South Asia). The regression coefficient of heavy-rainfall-day frequency on SWA is approximately opposite in sign to that of dry-spell-day frequency (Fig. 3b). In the historical simulations, changes in heavy-rainfall frequency are weakly related to SWA over continents, with increased frequency over South Asia and the Indochinese Peninsula. In RCP8.5, the relationship of heavy-rainfall-day frequency with SWA over South Asia is stronger than that in historical simulations. Furthermore, areas of significantly positive coefficients expand to western and southern China, the Indochinese Peninsula, and Japan, while areas of significantly negative coefficients cover Mexico, the central United States, and central Asia.

To investigate the intermodel spread of the relationship between hydrological extremes and SWA in historical and RCP8.5 simulations over these regions, we divide the subtropical continental band (15°–45°N) into six regions: North Africa–Middle East (NA-ME; 15°–30°N, 15°W–60°E), Mediterranean Europe (MED; 30°–45°N, 15°W–60°E), South Asia–East Asia (SA-EA; 15°–30°N, 60°–140°E), central Asia–East Asia (CA-EA; 30°–45°N, 60°–140°E), southern United States–Mexico (SUS-MEX; 15°–30°N, 125°–65°W), and northern United States (NUS; 30°–45°N, 125°–65°W). In these regions, we only use data over continents, and the values over oceans are masked. The results are not sensitive to shifting of longitudinal or latitudinal boundaries within 5°.

The strongest relationships are found over two regions, SUS-MEX and SA-EA (Fig. 4). Over SUS-MEX,

regression coefficients of dry-spell-day frequency are positive in 17 of 20 historical simulations, with a median of $5.0 \, \text{days} \, \mu^{-1}$, while all 20 RCP8.5 simulations show positive coefficients, with a median of $7.4 \, \text{days} \, \mu^{-1}$. This suggests that the increase in SWA is likely to associate with increase in number of dry-spell days over this region. The regression coefficients increase in 13 of 20 models between historical and RCP8.5 simulations (Fig. 4a). This indicates the SWA associated increase in number of dry spells is more likely than not to intensify in response of increased external forcing. The regression coefficients of heavy-rainfall-day frequency is negative in 17 of 20 historical simulations, with a median of $-0.64 \, \text{days} \, \mu^{-1}$, and negative in 16 of 20 RCP8.5, with a median of $-0.9 \, \text{days} \, \mu^{-1}$ (Fig. 4b). The regression coefficient decreases in 10 of 20 models between historical and RCP8.5 simulations. Thus it is likely that higher SWA relates to a decrease in number of heavy-rainfall days, but there is no evidence for a significant change in the relationship between SWA and heavy-rainfall days in this region.

Over SA-EA, the positive regression coefficient of heavy-rainfall-day frequency on SWA tends to increase from historical to RCP8.5 simulations. Regression coefficients of heavy-rainfall-day frequency are positive in 14 of 20 historical simulations, with a median of $0.32 \, \text{days} \, \mu^{-1}$, and 18 of 20 RCP8.5 simulations show positive coefficients, with a median of $1.0 \, \text{days} \, \mu^{-1}$. Thirteen of 20 models show increase in regression coefficients from historical to RCP8.5 (purple box for SA-EA in Fig. 4b). This suggests that higher SWA is likely associated with increased numbers of heavy-rainfall days over SA-EA, and this relationship is more likely than not to intensify from historical to RCP8.5. In the same region, the median regression coefficient of dry-spell-day frequency is $-3.8 \, \text{days} \, \mu^{-1}$ in historical simulations, dropping to $-5.2 \, \text{days} \, \mu^{-1}$ in RCP8.5. The regression coefficient decreases in 10 of 20 models between historical and RCP8.5 simulations (Fig. 4a); thus there is no evidence for a significant change in the relationship between SWA and dry days in the region.

Over NUS, positive regression coefficients of dry-spell-day frequency on SWA are found in 10 of 20 historical simulations, and 12 of 20 RCP8.5 simulations. Thirteen of 20 models show an increase in regression coefficients from the historical run to RCP8.5. This indicates that a positive relationship between the number of dry-spell days and SWA is more likely in RCP8.5 than in historical simulations over this region. In the same region, there is no significant evidence of a tendency toward either positive or negative regression coefficients of heavy-rainfall-day frequency on SWA. In the other three regions, the regional-mean regression coefficients

(a) Regression of dry-spell-day frequency on SWA
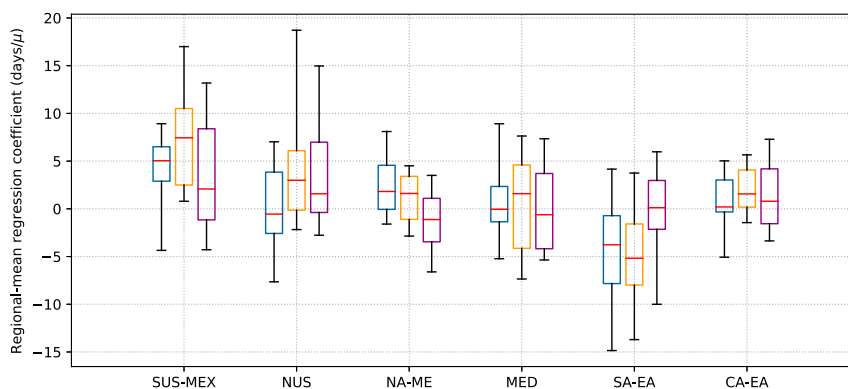
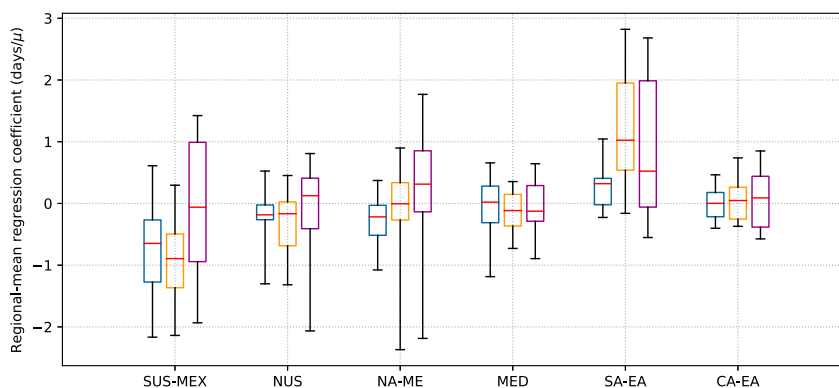(b) Regression of heavy-rainfall-day frequency on SWA

FIG. 4. Multimodel ensemble of regression coefficient between SWA and averaged number of (a) dry-spell days and (b) heavy-rainfall days over six regions—SUS-MEX (15°–30°N, 125°–65°W), NUS (30°–45°N, 125°–65°W), NA-ME (15°–30°N, 15°W–60°E), MED (30°–45°N, 15°W–60°E), SA-EA (15°–30°N, 60°–140°E), and CA-EA (30°–45°N, 60°–140°E)—for historical simulations (blue boxes), RCP8.5 simulations (orange boxes), and their differences (purple boxes). Red lines denote median values, boxes mark the 25%–75% likely range, and caps denote 5%–95% likely range.

are small, and there is no cross-model consensus on the sign of the relationships between the number of hydrological extremes and SWA.

The interannual relationships between SWA and hydrological extremes might be explained by dynamic processes: circulation anomalies associated with SWA could provide persistent weather conditions that favor the occurrence of hydrological extremes over these regions. To shed some light on this hypothesis, we examine regression coefficients of eddy streamfunction on SWA in both historical and RCP8.5 simulations. The multimodel mean regression coefficient is shown in Fig. 5 (shadings), superimposed with the multimodel mean climatology of the eddy streamfunction (Fig. 5, contours). The spatial patterns of climatology are

characterized by two strong high pressure centers over North Pacific and North Atlantic, one strong low pressure center over Eurasia, and one weak low pressure center over North America. These high pressure and low pressure centers represent ridges and troughs of stationary waves, respectively.

In both historical and RCP8.5 simulations, the regression coefficients indicate that increased SWA is related to strengthening of the Eurasian low pressure system, the North Pacific high pressure system, and the North Atlantic high pressure system, but weakening in the North American low pressure system. Since the climatological eddy streamfunction of the North American low is weaker by an order of magnitude than that of the other three pressure systems, the intensification in the
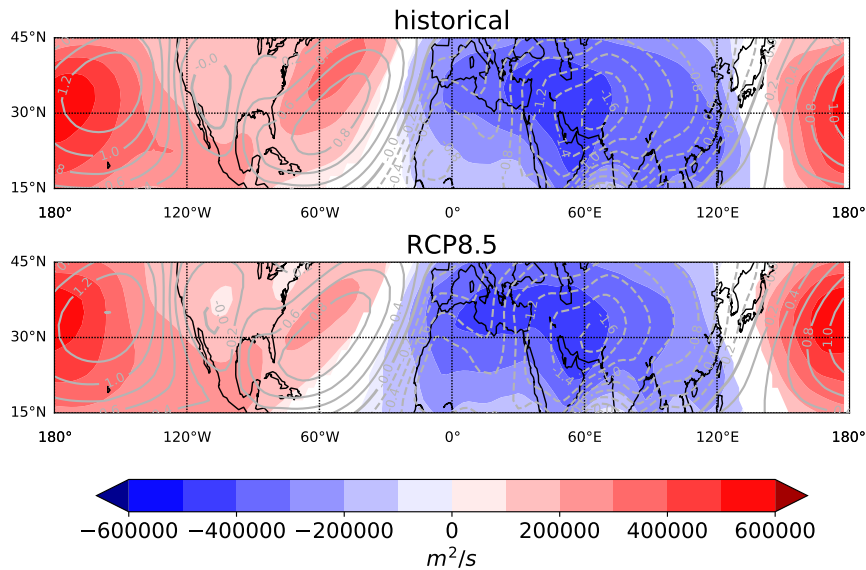
FIG. 5. The 20-model ensemble mean of climatological eddy streamfunction (contours) and regression coefficient of eddy streamfunction on SWA (shadings) in the last 50 years of (top) historical and (bottom) RCP8.5 simulations (units of contours: $10^7 \, \mathrm{m^2 \, s^{-1}}$). Warm (cool) colors denote positive (negative) values. Regression coefficients that are significant at the $p < 0.1$ level by the Student's t test are plotted.

amplitude of stationary waves is characterized by the strengthening of the three dominant pressure systems. In boreal summer, the summer monsoon is a dominant factor that brings moisture from the Indian Ocean to the SA-EA region, fueling precipitation. The strengthening of the Eurasian low pressure system likely reflects intensification of the monsoonal flow over the SA-EA region. By increasing moisture transport, this intensification would favor more frequent occurrence of heavy rainfall over EA-SA during periods of large SWA. At the same time, the expansion of North Atlantic and North Pacific high pressure systems, along with the weakening of the North American low pressure system, indicates decreased moisture transport and increased subsidence over the United States and Mexico, which favor occurrences of dry spells.

d. Contribution on projected changes in number of hydrological extremes

Since global warming is known to be a major contributor to projected increases in hydrological extremes, we use a multiple linear regression model that accounts for two explanatory variables—SWA and global mean surface temperature (GMT)—to separate the influence of global warming on hydrological extremes from the interannual relationships between SWA and the number of hydrological extremes. The multiple linear regression coefficients of the number of hydrological extremes on both the normalized SWA and GMT

anomaly in JJA during the last 50 years of both historical and RCP8.5 scenarios for each model are obtained using the ordinary least squares estimate:

$$n_i(x, y) = R_{SWA}(x, y)NSWA_i + R_{GMT}(x, y)NGMT_i$$
$$+ \alpha + \varepsilon_i, \qquad (2)$$

where n, i, ε, x, and y are the same as in Eq. (1). The terms $R_{SWA}(x, y)$ and $R_{GMT}(x, y)$ are the regression coefficients of SWA and GMT, respectively; α is the intercept and NGMT represents the anomaly with respect to the model's climatological-mean GMT in PiControl. Patterns of R_{SWA} (Figs. 6a,b) are similar to patterns of linear regression coefficients on SWA alone (Fig. 3) in both scenarios. The R_{GMT} values (Figs. 6c,d) are much smaller than R_{SWA}. These results indicate although global warming may play an important role in the projected increase in the frequency of hydrological extremes, GMT is not strongly correlated with regional hydrological extremes on an interannual time scale, over which SWA is significantly related to number of hydrological extremes over certain regions.

We employ the multiple linear regression coefficient in RCP8.5 to produce an initial assessment of the portion of the projected changes in hydrological extremes that can be explained by intensification of SWA alone by the end of this century. First, we examine the multimodel ensemble mean of projected changes in the climatological

(a) Multiple linear regression of dry-spell-day frequency on SWA

(b) Multiple linear regression of heavy-rainfall-day frequency on SWA

(c) Multiple linear regression of dry-spell-day frequency on GMT

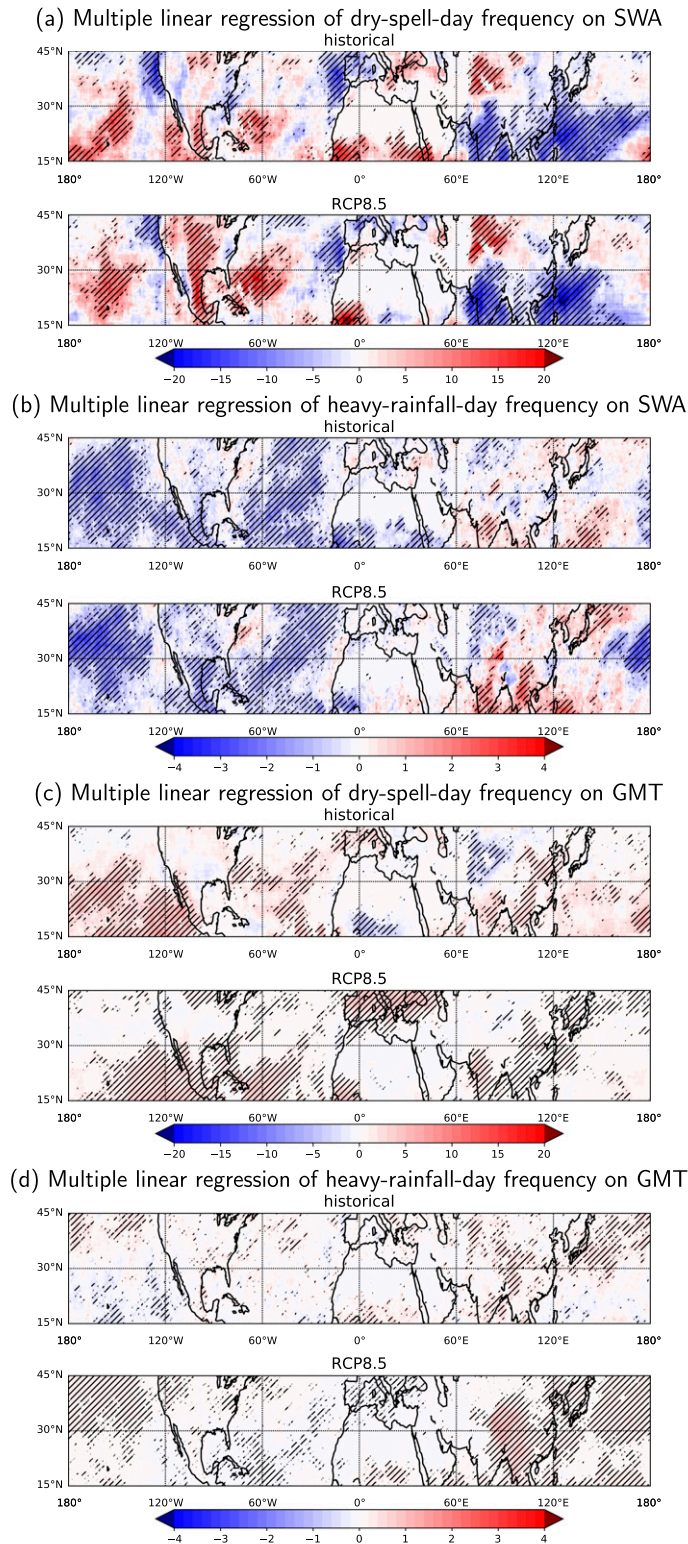(d) Multiple linear regression of heavy-rainfall-day frequency on GMT

FIG. 6. Multimodel mean of the multiple linear regression coefficient (units are days μ^{-1} for SWA and days K^{-1} for GMT) of interannual variability in the number of hydrological extremes on SWA and GMT: (a) number of dry-spell days on SWA, (b) number of heavy-rainfall days on SWA, (c) number of dry-spell days on GMT, and (d) number of heavy-rainfall days on GMT. Warm (cool) colors denote positive (negative) values. Hatched areas denote values are significant at $p < 0.1$ level by the Student's t test.

number of hydrological extremes in summer from the period of 1956–2005 in historical to the period of 2050–99 in RCP8.5, which we define as δn. We focus on the multimodel ensemble mean to increase the ratio of forced signal to internal variability. Over the continents, the δn of dry-spell days is significantly ($p < 0.1$ by the Student's t test) positive over the northwestern and central United States, Mexico, the Mediterranean, South Asia, East Asia, and the Indochinese Peninsula (Fig. 7a). The δn of heavy-rainfall days is significantly positive over South Asia, northwestern China, and Indochinese Peninsula (Fig. 7b).

Second, we estimate δn_{SWA}, the changes in number of hydrological extremes predicted by changing SWA from historical to RCP8.5 but holding GMT unchanged:

$$\delta n_{\mathrm{SWA}}(x, y) = R_{\mathrm{SWA\_RCP85}}(x, y)$$
$$\times (\overline{\mathrm{NSWA}_{\mathrm{RCP85}}} - \overline{\mathrm{NSWA}_{\mathrm{hist}}}), \quad (3)$$

where $R_{\mathrm{SWA\_RCP85}}$ is the regression coefficient on NSWA in RCP8.5; $\overline{\mathrm{NSWA}_{\mathrm{hist}}}$ represents the average of the NSWA index over the period 1956–2005 for historical simulations, and $\overline{\mathrm{NSWA}_{\mathrm{RCP85}}}$ indicates the average of NSWA index over the period 2051–2100 for RCP8.5 simulations. We similarly estimate the changes in number of hydrological extremes that are predicted by the change in average GMT from historical to RCP8.5 but holding SWA unchanged (δn_{GMT}):

$$\delta n_{\mathrm{GMT}}(x, y) = R_{\mathrm{GMT\_RCP85}}(x, y)$$
$$\times (\overline{\mathrm{NGMT}_{\mathrm{RCP85}}} - \overline{\mathrm{NGMT}_{\mathrm{hist}}}). \quad (4)$$

Here, $R_{\mathrm{GMT\_RCP85}}$ is the regression coefficient on NGMT in RCP8.5. Note that $\overline{\mathrm{NGMT}_{\mathrm{RCP85}}}$ and $\overline{\mathrm{NGMT}_{\mathrm{hist}}}$ are calculated in manner that parallels that of $\overline{\mathrm{NSWA}_{\mathrm{RCP85}}}$ and $\overline{\mathrm{NSWA}_{\mathrm{hist}}}$ in Eq. (3), but for GMT.

The spatial pattern of the multimodel mean δn is similar to that of δn_{GMT} (Fig. S2), except for some regions where δn_{SWA} explains a substantial portion of changes in hydrological extremes (Fig. 7). Intensification of SWA predicts significantly positive δn_{SWA} of dry-spell days over eastern Mexico and northwestern and central United States (Fig. 7a), complementing the GMT-driven increase in number of dry-spell days over the midwestern United States and Mexico (Fig. S2a). Over SA-EA, SWA amplification reduces the number of dry spells (Fig. 7a), partially offsetting a positive δn_{GMT} of dry spells over this region (Fig. S2a). On the other hand, intensification of SWA generates significantly ($p < 0.1$ by the Student's t test) positive δn_{SWA} of heavy-rainfall days over India, southern China, and the Indochinese Peninsula (Fig. 7b), supplementing

the positive δn_{GMT} of heavy-rainfall days over the same regions (Fig. S2b). To assess the relative contributions of δn_{SWA} to δn, we examine the ratio $\delta n_{\mathrm{SWA}}/\delta n$ (Fig. 8a). For dry-spell days, the positive δn_{SWA} observed in Fig. 7a is generally over 10% of δn in most areas of NUS and eastern Mexico, and exceeds 30% of δn at some places in these regions, such as Northern California and Oregon (Fig. 8a). Over SA-EA, the δn_{SWA} of dry-spell days is opposite in sign to δn of dry-spell days and generally above 20% in magnitude (Fig. 8a). For heavy-rainfall days, the positive δn_{SWA} observed in Fig. 7b is above 10% of δn over most areas of SA-EA, and exceeds 20% at some places over western India (Fig. 8a).

To assess the combined effect of changes in SWA and changes in the relationships between number of hydrological extremes and SW, we define the changes in number of hydrological extremes that are predicted by concurrent changes in R_{SWA} and SWA as

$$\delta n_{\mathrm{SWA} \times R}(x, y) = R_{\mathrm{SWA\_RCP85}}(x, y) \times \overline{\mathrm{NSWA}_{\mathrm{RCP85}}}$$
$$- R_{\mathrm{SWA\_hist}}(x, y) \times \overline{\mathrm{NSWA}_{\mathrm{hist}}},$$

where $R_{\mathrm{SWA\_hist}}$ is the regression coefficient in historical. The multimodel mean of $\delta n_{\mathrm{SWA} \times R}$ has a similar pattern to but is larger in magnitude than the multimodel mean of δn_{SWA} (Fig. 7). Specifically, $\delta n_{\mathrm{SWA} \times R}$ of dry-spell days is significantly positive over eastern Mexico and northwestern and central United States (Fig. 7a), in most areas exceeding 30% of δn (Fig. 8b). The positive $\delta n_{\mathrm{SWA} \times R}$ of heavy-rainfall days exceeds 30% of δn over most areas of India, the Indochinese Peninsula, and southern China (Fig. 8b). These results indicate that the amplification of SWA, combined with the intensifying relationship of SWA with hydrological extremes, might explain a larger fraction of increases in number of dry-spell days over eastern Mexico and northwestern and central United States, and increases in heavy-rainfall days over India, the Indochinese Peninsula, and southern China than does the amplification of SWA alone.

4. Discussion and conclusions

In this study, we use simulations in three scenarios from 31 CMIP5 GCMs to investigate whether boreal-summer subtropical stationary waves are amplified in response to increased forcing, and whether a positive trend of SWA, such as that observed over 1979–2013, is more likely under external forcing than in the absence of forcing. Our results suggest that the climatological mean SWA increases in 29 of 31 simulations from PiControl to
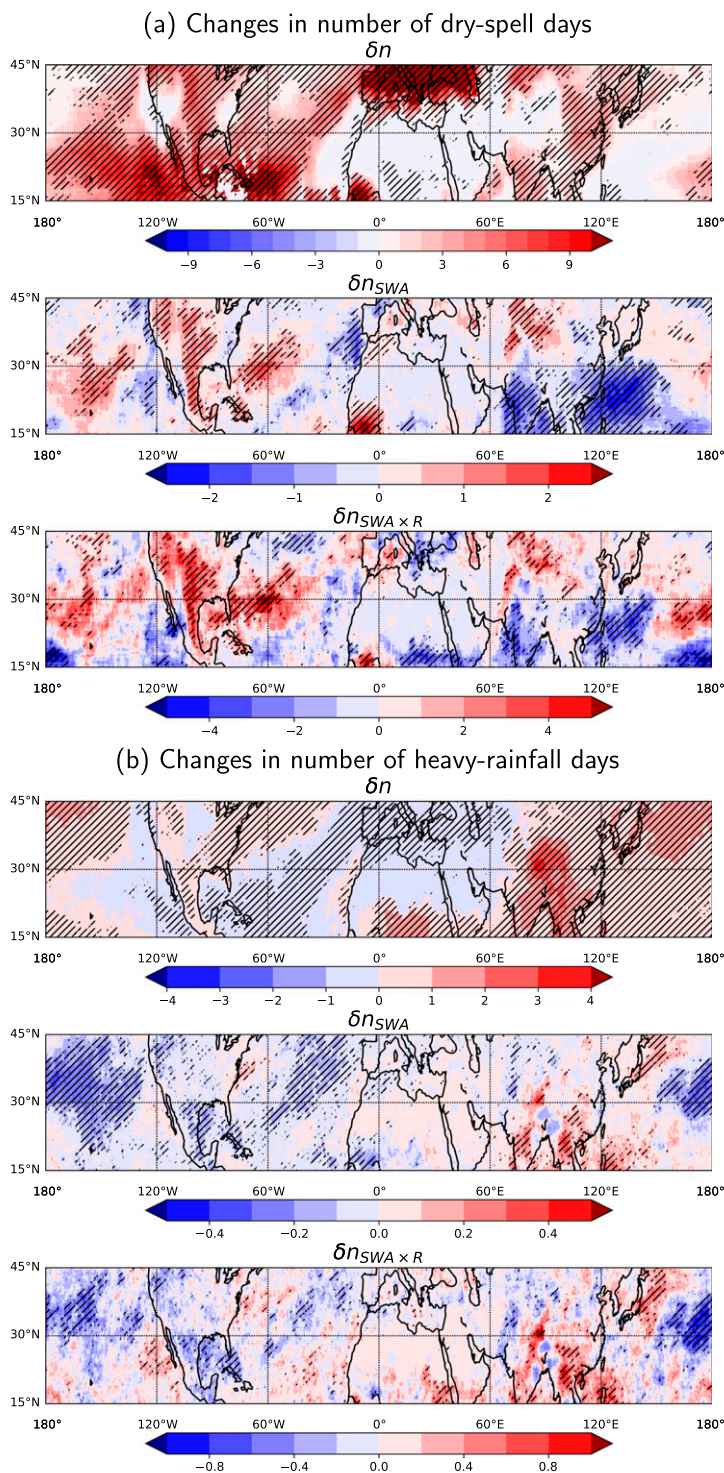
FIG. 7. Multimodel mean of changes in projected number of hydrological extremes (δn), changes in predicted number of hydrological extremes explained by changes in SWA alone (δn_{SWA}), and changes in predicted number of hydrological extremes explained by changes in both SWA and regression coefficient between SWA and hydrological extremes ($\delta n_{\mathrm{SWA} \times R}$) from historical to RCP8.5 for (a) dry-spell days and (b) heavy-rainfall days (unit is days). Warm (cool) colors denote positive (negative) values. Hatched areas denote values are significant at the $p < 0.1$ level by the Student's t test. Note changes in the scale of color bars between panels.
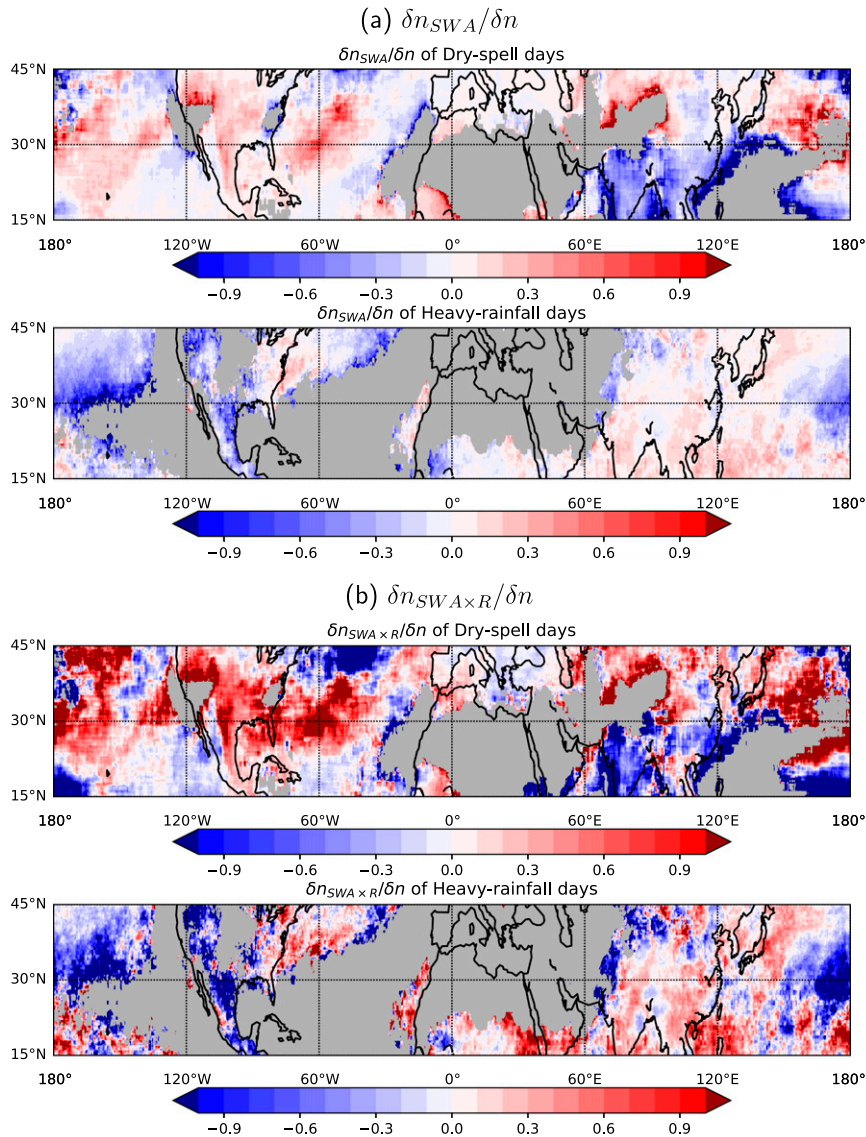
FIG. 8. (a) The $\delta n_{\mathrm{SWA}}/\delta n$ and (b) $\delta n_{\mathrm{SWA}\times R}/\delta n$ in Fig. 7. Warm (cool) colors denote positive (negative) values. Gray shadings mask areas where δn is close to zero.

historical, and in 26 of 31 simulations from historical to RCP85. There are 24 of 31 models showing a continuous increase in climatological mean SWA in response to increasing external forcing. The probability distribution of SWA trends in the absence of forcing shows neither a positive nor a negative tendency, but 22 of 31 models show positive SWA trends in historical simulations, and 26 of 31 show positive trends in response to the even stronger positive forcing in RCP8.5 simulations. These results suggest that the observed positive trend of SWA has been made more likely as a result of positive anthropogenic forcing.

Summer is the peak season of crop growth and human travel, and so summer hydrological extremes have particularly large potential for damage to agriculture and tourism (Rosenzweig et al. 2001; Amelung et al. 2007). This study assesses the relationship between stationary waves and number of hydrological extremes in summer. The regression results suggest that positive SWA anomalies are related to the increased number of heavy-rainfall days and decreased frequency of dry-spell days over SA–EA, as well as the increased number of dry-spell days over the United States and Mexico. Our hypothesis is that the interannual relationships between SWA and number of hydrological extremes might be explained by dynamic processes, specifically that changes in circulation associated with the SWA anomaly can provide persistent weather conditions that favor the occurrence of hydrological extremes over these regions.

The regression of the eddy streamfunction on SWA (section 3c) provides some evidence to support this hypothesis. The results of this regression show that positive amplitude anomalies of stationary waves relate to deepening of the Eurasian low and strengthening of the North Pacific high and the North Atlantic high, which could provide persistent local conditions that favor hydrological extremes over these regions. For example, these pressure anomalies could lead to a strengthened monsoon over India and southern China, as well as weakening convergence and moisture transport over the United States and Mexico.

These relationships between SWA and number of hydrological extremes are more likely than not to change in response to external forcing. The strongest signals are over SA-EA, SUS-MEX, and NUS. Thirteen of 20 models show the intensification from historical to RCP8.5 in relationships between the number of heavy-rainfall days and SWA over SA-EA, and between the number of dry-spell days and SWA over SUS-MEX and NUS. The intensification of these interannual relationships might be explained by thermodynamic processes, specifically the increase in atmospheric moisture content in a warmer atmosphere. As suggested by Held and Soden (2006), assuming the circulation of stationary waves remain unchanged, the substantial increase in the moisture content of the atmosphere with warming would enhance the transport of water vapor by the atmospheric circulation from regions of water vapor divergence to regions of water vapor convergence, so that dry regions get drier and wet regions get wetter. In other words, stationary waves play an important role in redistributing increased water vapor in a warm climate. Further studies are needed to understand details of mechanisms that link SWA to regional hydrological extremes and mechanisms that cause changes in relationships between SWA and hydrological extremes in response to external forcing.

The multiple linear regression results suggest that relationships between SWA and number of hydrological extremes in some subtropical regions are significant and not driven by an increase in global mean temperature. Furthermore, projected changes in the number of hydrological extremes can be partially explained by intensification of SWA from historical to RCP8.5, with the regression coefficient remained unchanged. Specifically, intensification of SWA may explain above 10% (exceeding 30% at some places) of the projected increase in the number of dry spells over the United States and Mexico and above 10% (exceeding 20% at some places) of the projected increase in number of heavy-rainfall days over India, the Indochinese Peninsula, and southern China. Further, considering the changing relationships

between the number of hydrological extremes and SWA suggests an even larger role for subtropical stationary waves in explaining the projected increase in the number of hydrological extremes from historical to RCP8.5 over these regions.

REFERENCES

Adams, D. K., and A. C. Comrie, 1997: The North American monsoon. *Bull. Amer. Meteor. Soc.*, **78**, 2197–2214, https://doi.org/10.1175/1520-0477(1997)078<2197:TNAM>2.0.CO;2.

Amelung, B., S. Nicholls, and D. Viner, 2007: Implications of global climate change for tourism flows and seasonality. *J. Travel Res.*, **45**, 285–296, https://doi.org/10.1177/0047287506295937.

Aon Benfield, 2016: Global Catastrophe Recap: August 2016. Aon Benfield, 18 pp., http://thoughtleadership.aonbenfield.com/Documents/20160908-ab-analytics-if-august-global-recap.pdf.

Chen, T.-C., 2003: Maintenance of summer monsoon circulations: A planetary-scale perspective. *J. Climate*, **16**, 2022–2037, https://doi.org/10.1175/1520-0442(2003)016<2022:MOSMCA>2.0.CO;2.

Collins, M., and Coauthors, 2013: Long-term climate change: Projections, commitments and irreversibility. *Climate Change 2013: The Physical Science Basis.* T. F. Stocker et al., Eds., Cambridge University Press, 1029–1136, http://www.climatechange2013.org/images/report/WG1AR5_Chapter12_FINAL.pdf.

Coumou, D., V. Petoukhov, S. Rahmstorf, S. Petri, and H. J. Schellnhuber, 2014: Quasi-resonant circulation regimes and hemispheric synchronization of extreme weather in boreal summer. *Proc. Natl. Acad. Sci. USA*, **111**, 12 331–12 336, https://doi.org/10.1073/pnas.1412797111.

Dai, A., 2011: Drought under global warming: A review. *Wiley Interdiscip. Rev.: Climate Change*, **2**, 45–65, https://doi.org/10.1002/wcc.81.

Davis, R. E., B. P. Hayden, D. A. Gay, W. L. Phillips, and G. V. Jones, 1997: The North Atlantic subtropical anticyclone. *J. Climate*, **10**,

728–744, https://doi.org/10.1175/1520-0442(1997)010<0728:TNASA>2.0.CO;2.

Donat, M. G., and Coauthors, 2013: Updated analyses of temperature and precipitation extreme indices since the beginning of the twentieth century: The HadEX2 dataset. *J. Geophys. Res. Atmos.*, **118**, 2098–2118, https://doi.org/10.1002/jgrd.50150.

Efron, B., and R. J. Tibshirani, 1994: *An Introduction to the Bootstrap*. CRC Press, 456 pp.

Grams, C. M., H. Binder, S. Pfahl, N. Piaget, and H. Wernli, 2014: Atmospheric processes triggering the central European floods in June 2013. *Nat. Hazards Earth Syst. Sci.*, **14**, 1691–1702, https://doi.org/10.5194/nhess-14-1691-2014.

Held, I. M., and B. J. Soden, 2006: Robust responses of the hydrological cycle to global warming. *J. Climate*, **19**, 5686–5699, https://doi.org/10.1175/JCLI3990.1.

Holton, J. R., and G. J. Hakim, 2012: *An Introduction to Dynamic Meteorology*. 5th ed. Academic Press, 552 pp.

Kohyama, T., D. L. Hartmann, and D. S. Battisti, 2017: La Niña–like mean-state response to global warming and potential oceanic roles. *J. Climate*, **30**, 4207–4225, https://doi.org/10.1175/JCLI-D-16-0441.1.

Lehmann, J., D. Coumou, and K. Frieler, 2015: Increased record-breaking precipitation events under global warming. *Climatic Change*, **132**, 501–515, https://doi.org/10.1007/s10584-015-1434-y.

Levine, X. J., and W. R. Boos, 2016: A mechanism for the response of the zonally asymmetric subtropical hydrologic cycle to global warming. *J. Climate*, **29**, 7851–7867, https://doi.org/10.1175/JCLI-D-15-0826.1.

Li, W., L. Li, R. Fu, Y. Deng, and H. Wang, 2011: Changes to the North Atlantic subtropical high and its role in the intensification of summer rainfall variability in the southeastern United States. *J. Climate*, **24**, 1499–1506, https://doi.org/10.1175/2010JCLI3829.1.

Liu, J., J. A. Curry, H. Wang, M. Song, and R. M. Horton, 2012: Impact of declining Arctic sea ice on winter snowfall. *Proc. Natl. Acad. Sci. USA*, **109**, 4074–4079, https://doi.org/10.1073/pnas.1114910109.

Lu, J., L. R. Leung, Q. Yang, G. Chen, W. D. Collins, F. Li, Z. J. Hou, and X. Feng, 2014: The robust dynamical contribution to precipitation extremes in idealized warming simulations across model resolutions. *Geophys. Res. Lett.*, **41**, 2971–2978, https://doi.org/10.1002/2014GL059532.

Mann, M. E., S. Rahmstorf, K. Kornhuber, B. A. Steinman, S. K. Miller, and D. Coumou, 2017: Influence of anthropogenic climate change on planetary wave resonance and extreme weather events. *Sci. Rep.*, **7**, 45242, https://doi.org/10.1038/srep45242.

Mehran, A., A. AghaKouchak, and T. J. Phillips, 2014: Evaluation of CMIP5 continental precipitation simulations relative to satellite-based gauge-adjusted observations. *J. Geophys. Res. Atmos.*, **119**, 1695–1707, https://doi.org/10.1002/2013JD021152.

Miyasaka, T., and H. Nakamura, 2005: Structure and formation mechanisms of the Northern Hemisphere summertime subtropical highs. *J. Climate*, **18**, 5046–5065, https://doi.org/10.1175/JCLI3599.1.

Nigam, S., and E. DeWeaver, 2003: Stationary waves (orographic and thermally forced). *Encyclopedia of Atmospheric Sciences*, J. R. Holton, Ed., Academic Press, 2121–2137 http://www.atmos.umd.edu/~nigam/Encyc.Atmos.Sci.Stationary.Waves.Nigam-DeWeaver.2003.pdf.

NOAA, 2017: Global Climate Report–Annual 2016. NOAA/NCEI, accessed 10 May 2018, https://www.ncdc.noaa.gov/sotc/global/201613.

O'Gorman, P. A., and T. Schneider, 2009a: The physical basis for increases in precipitation extremes in simulations of 21st-century climate change. *Proc. Natl. Acad. Sci. USA*, **106**, 14 773–14 777, https://doi.org/10.1073/pnas.0907610106.

——, and ——, 2009b: Scaling of precipitation extremes over a wide range of climates simulated with an idealized GCM. *J. Climate*, **22**, 5676–5685, https://doi.org/10.1175/2009JCLI2701.1.

Pall, P., M. R. Allen, and D. A. Stone, 2007: Testing the Clausius–Clapeyron constraint on changes in extreme precipitation under CO_2. *Climate Dyn.*, **28**, 351–363, https://doi.org/10.1007/s00382-006-0180-2.

Petoukhov, V., S. Rahmstorf, S. Petri, and H. J. Schellnhuber, 2013: Quasiresonant amplification of planetary waves and recent Northern Hemisphere weather extremes. *Proc. Natl. Acad. Sci. USA*, **110**, 5336–5341, https://doi.org/10.1073/pnas.1222000110.

Rodwell, M. J., and B. J. Hoskins, 2001: Subtropical anticyclones and summer monsoons. *J. Climate*, **14**, 3192–3211, https://doi.org/10.1175/1520-0442(2001)014<3192:SAASM>2.0.CO;2.

Rosenzweig, C., A. Iglesias, X. B. Yang, P. R. Epstein, and E. Chivian, 2001: Climate change and extreme weather events: Implications for food production, plant diseases, and pests. *Global Change Hum. Health*, **2**, 90–104, https://doi.org/10.1023/A:1015086831467.

Screen, J. A., and I. Simmonds, 2014: Amplified mid-latitude planetary waves favour particular regional weather extremes. *Nat. Climate Change*, **4**, 704–709, https://doi.org/10.1038/nclimate2271.

Seager, R., N. Naik, and G. A. Vecchi, 2010: Thermodynamic and dynamic mechanisms for large-scale changes in the hydrological cycle in response to global warming. *J. Climate*, **23**, 4651–4668, https://doi.org/10.1175/2010JCLI3655.1.

Sheffield, J., G. Goteti, and E. F. Wood, 2006: Development of a 50-year high-resolution global dataset of meteorological forcings for land surface modeling. *J. Climate*, **19**, 3088–3111, https://doi.org/10.1175/JCLI3790.1.

Sillmann, J., V. V. Kharin, X. Zhang, F. W. Zwiers, and D. Bronaugh, 2013: Climate extremes indices in the CMIP5 multimodel ensemble: Part 1. Model evaluation in the present climate. *J. Geophys. Res. Atmos.*, **118**, 1716–1733, https://doi.org/10.1002/jgrd.50203.

Simpson, I. R., R. Seager, M. Ting, and T. A. Shaw, 2016: Causes of change in Northern Hemisphere winter meridional winds and regional hydroclimate. *Nat. Climate Change*, **6**, 65, https://doi.org/10.1038/nclimate2783.

Sun, Y., S. Solomon, A. Dai, and R. W. Portmann, 2007: How often will it rain? *J. Climate*, **20**, 4801–4818, https://doi.org/10.1175/JCLI4263.1.

Taylor, K. E., R. J. Stouffer, and G. A. Meehl, 2012: An overview of CMIP5 and the experiment design. *Bull. Amer. Meteor. Soc.*, **93**, 485–498, https://doi.org/10.1175/BAMS-D-11-00094.1.

Thrasher, B., E. P. Maurer, C. McKellar, and P. B. Duffy, 2012: Technical note: Bias correcting climate model simulated daily temperature extremes with quantile mapping. *Hydrol. Earth Syst. Sci.*, **16**, 3309–3314, https://doi.org/10.5194/hess-16-3309-2012.

Ting, M., 1994: Maintenance of northern summer stationary waves in a GCM. *J. Atmos. Sci.*, **51**, 3286–3308, https://doi.org/10.1175/1520-0469(1994)051<3286:MONSSW>2.0.CO;2.

Trenberth, K. E., A. Dai, R. M. Rasmussen, and D. B. Parsons, 2003: The changing character of precipitation. *Bull. Amer.*

Meteor. Soc., **84**, 1205–1218, https://doi.org/10.1175/BAMS-84-9-1205.

Vahedifard, F., A. AghaKouchak, and N. H. Jafari, 2016: Compound hazards yield Louisiana flood. *Science*, **353**, 1374, https://doi.org/10.1126/science.aai8579.

Wills, R. C., and T. Schneider, 2015: Stationary eddies and the zonal asymmetry of net precipitation and ocean freshwater forcing. *J. Climate*, **28**, 5115–5133, https://doi.org/10.1175/JCLI-D-14-00573.1.

——, and ——, 2016: How stationary eddies shape changes in the hydrological cycle: Zonally asymmetric experiments in an idealized GCM. *J. Climate*, **29**, 3161–3179, https://doi.org/10.1175/JCLI-D-15-0781.1.

——, M. P. Byrne, and T. Schneider, 2016: Thermodynamic and dynamic controls on changes in the zonally anomalous hydrological cycle. *Geophys. Res. Lett.*, **43**, 4640–4649, https://doi.org/10.1002/2016GL068418.

Yuan, J., W. Li, and Y. Deng, 2015: Amplified subtropical stationary waves in boreal summer and their implications for regional water extremes. *Environ. Res. Lett.*, **10**, 104009, https://doi.org/10.1088/1748-9326/10/10/104009.

Zhang, X., H. Wan, F. W. Zwiers, G. C. Hegerl, and S.-K. Min, 2013: Attributing intensification of precipitation extremes to human influence. *Geophys. Res. Lett.*, **40**, 5252–5257, https://doi.org/10.1002/grl.51010.